# Intrinsic Evolution on the Decoupling-Coupling-Decoupling of the plasma Density and Temperature profiles in a Cylindrical Laboratory Plasma Device

C.Y. Wang,[1] W.W. Xiao,[1, a)] Y. Ren,[2] W.L. Zhong,[3] G.L. Xiao,[3] X.L. Zou,[4] P.H. Diamond,[5] G.R. Tynan,[5] X.B. Peng,[6] J.T. Ma,[1] J. Wu,[1] Z.H. Wang,[3] X.Q. Ji,[3] Z.C. Yang,[3] J.Q. Dong,[3] and X.T. Ding[3]

[1)] *IFTS, Department of Physics, Zhejiang University, Hangzhou, 310027, China*

[2)] *PPPL, Princeton University, P.O. Box 451, Princeton, New Jersey 08543, USA*

[3)] *Southwestern Institute of Physics, P.O. Box 432, Chengdu, China*

[4)] *CEA, IRFM, F-13108 Saint-Paul-lez-Durance, France*

[5)] *Center for Energy Research, University of California San Diego, La Jolla, CA 92093, USA*

[6)] *Institute of Plasma Physics, Chinese Academy of Sciences, Hefei Anhui, 230031, China*

(Dated: 19 April 2022)

An intrinsic evolution on the decoupling-coupling-decoupling (DCD) of the electron density and temperature profiles responding to the magnetic field change in a cylindrical laboratory plasma device is reported with no external particle, heating and momentum source. Experimental results show that the density and the temperature profiles decouple with low magnetic field, couple with higher magnetic field and decouple again with the continuous magnetic field increase. An element physical picture of the DCD regime is unraveled based on the analyses of gradient lengths, the turbulence propagation directions and the turbulence spatial scales, and the relationship between the normalized collision rates and the poloidal mode numbers.

As significant physics, the coupling and the decoupling are widely studied in the super-Alfvénic space plasma expansion[1–3], the inertial confinement fusion (ICF) on the enhanced energy coupling[4,5] and the pulsed inductive thrusters (PIT) between the accelerator coil magnetic field and the plasma[6,7]. In the magnetically confinement fusion (MCF) field, since first being observed on sawtooth oscillations[8], the coupling and the decoupling physics have also been researched for a long history[9–13]. The coupling and the decoupling are extensive and important physics in magnetized plasma, in particular, the experimental instigations on the high confinement mode (H-mode)[14–16] and the improved energy confinement mode (I-mode)[17–20] show that the coupling and the decoupling between the density profiles and the temperature profiles are observed in tokamaks. Since the H-mode and the I-mode are still potential operational regimes for the future fusion power approaches, the fundamental physics of the coupling and the decoupling of the density and the temperature profiles is still necessary to studied using a few systematic methods.

In this work, we report *three* distinct observations that taken together show that those previous experimental results on edge profiles coupling and decoupling phenomena in H-mode and I-mode can be refined by an intrinsic evolution on the decoupling-coupling-decoupling (DCD) in a cylindrical laboratory plasma device. *First*, the temperature gradient is almost no change while the density gradient increases with the magnetic field increase 0.5 kGs to 0.8 kGs, then both density and temperature gradients increase from 0.8 kGs to 1.1 kGs, and then the density gradient is almost no change while the temperature gradient increases with the magnetic field increase from 1.1 kGs to 2 kGs. *Second*, the propagation directions of the

[a)] Electronic mail: wwxiao@zju.edu.cn

poloidal wavenumber ($k_\theta$) and the radial wavenumber ($k_r$) with magnetic fields changes are different, and the drift wave (DW)[21] extends to higher frequency region. *Third*, the density gradients drive a nonlinear change of the density fluctuations with magnetic fields increase, and the integral density decreases while the integral temperature increases. Meanwhile, the relationship between the normalized collision rates of the electron to electron ($\upsilon^*_{ee}$) and the poloidal mode numbers ($m$) at r=4.5cm is strongly related to the density. This means that one potential mechanism affects density, which induces the DCD regime of the density and the temperature. We also statistically analyze a few tokamaks with H-mode and I-mode plasmas on the $\upsilon^*_{ee}$ and the $m$. A comparison result shows that the intrinsic evolution on the DCD regime is similar to the previous cases with the H-mode and the I-mode plasmas since the density could be the key parameter of the H-mode versus to the I-mode with almost fixed heating power. Thus, the issue to the density effect is the element on the intrinsic evolution on the DCD regime in the cylindrical laboratory plasmas, this is significantly helpful to understand the observations of the density and the temperature coupling and decoupling associated with the H-mode and I-mode plasmas in tokamaks.

The experiments reported were carried on the Zheda Plasma Experimental Device(ZPED)[22], which is a cylindrical magnetized plasma device at Zhejiang University. The size of the vacuum chamber is 2.0m in length and 0.3m in diameter. The Nitrogen plasma is produced by a 13.56MHz radio frequency (RF) source with 200W forward and 20W reflect power.

The Quadruple Langmuir probe(QLP)[23] and the Langmuir rake probes are the key diagnostics for the plasma profiles, the density fluctuations. A diagram of QLP is shown in Fig. 1 (a). It consists of four tungsten tips, 1, 2, 3 and 4 of 1cm in length and 1.4mm in diameter. The distance between the tips along the poloidal direction is 4.6 mm between tip3 and tip4. The distance between the tip1 and tip2 along the magnetic field direction is 4.5 mm, as shown in Figure 1 (a). The plasma profiles (electron density, electron temperature), the density fluctuation and the poloidal wavenumbers ($k_\theta$) are measured by the QLP. A diagram of the Langmuir rake probe is shown in Figure 1 (b). It consists of 12 tungsten tips in the radial direction from center to the edge of the plasma. The length and the diameter of each tip are 2mm and 2mm, respectively. The distance between two adjacent tips is 4mm. The radial wavenumbers ($k_r$) are measured by the Langmuir rake probe. The magnetic field direction, the QLP and the Langmuir rake probe moving directions are marked in Figure 1 by the arrows. In this work, all of the poloidal mode numbers ($m$) are measured by the fast camera diagnostic[24].

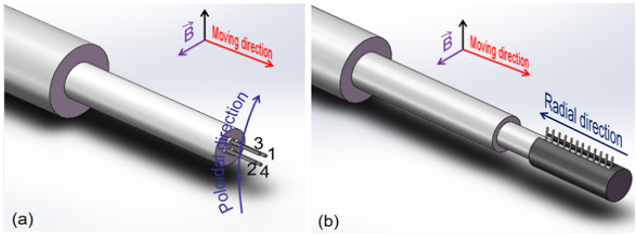


FIG. 1. (a) is the diagram of QLP and (b) is the diagram of Langmuir rake probe. The magnetic field direction, the poloidal direction and the moving direction are indicated by the arrows.

The density and the temperature profiles with different magnetic fields are measured by the QLP as shown in Figure 2 (a) and (b), respectively. Here, a key analysis region is around at $r = 4.5cm$ (by the red line). The ionization of the neutral gas is estimated by the Saha equation[25] $a^2/(1-a^2) = (2.4 \times 10^{-4}/p)T^{2.5}e^{-u/KT}$. The ionization number $a$ is about 99%, very close to full ionization. Here, the thermodynamic temperature ($T$) is about $3 \times 10^4 K$, the ionization energy ($u$) of nitrogen atom is 14.5 eV, the plasma temperature ($KT$) is about 3eV, and the pressure ($p$) is about 1.5mtorr.

Based on Figure 2, a detailed analysis of the gradient is shown in Figure 3. The density gradient length ($1/L_{n_e} = \Delta n_e/n_e$) and the temperature gradient length ($1/L_{T_e} = \Delta T_e/T_e$) are shown by the blue curve and the red curve, respectively. The density gradient increases

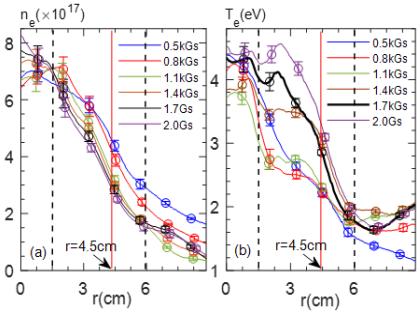


FIG. 2. (a) and (b) are the density profiles and the temperature profiles, respectively. The main analysis region is at $r = 4.5cm$, as shown by the red line. The black dashed lines represent the regions of the integral density and the integral temperature, which will be discussed in Figure 4.

with the magnetic field increase, while the temperature gradient almost no change in region I; the density gradient continuously increases, meanwhile the temperature gradient increases with the magnetic increase as well in region II; however, the temperature gradient increases with the magnetic field increase but the density gradient almost no change in region III. This means that the DCD regime exists with the magnetic field increase: the density profile and the temperature profile are decoupled in region I, density gradient increases without the temperature profile no change; the density and the temperature are coupled in region II, both the density gradient and the temperature gradient increase together; the density and the temperature are decoupled, the temperature gradient increases with flat density gradient in region III.

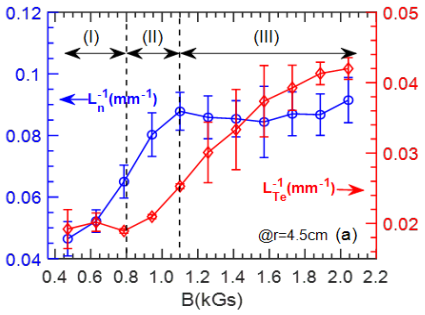


FIG. 3. the distributions of the $1/L_n$ and the $1/L_{Te}$ at $r = 4.5cm$ with magnetic field increase. The three regions of the DCD regime are separated by the gradient changes of the density and the temperature.

In each region, the fundamental physics of the DCD regime related to the wavenumber spectra and the density fluctuation are also analyzed, as shown in figure 4. The poloidal and the radial wavenumber spectra are obtained according to the two-point correlation method[26,27], and the cross power spectra of floating voltage measured by two floating probes are derived with $C^j_{XY} = X^j(f)Y^{j*}(f) = Ae^{i\cdot\theta_j(f)}$, where $j$ is the number of samples, $X$ and $Y$ are the Fourier transform of floating voltage, $*$ denotes the complex conjugation. The wavenumber $k_j$ is confirmed by the phase difference $\theta_j$, $k_j(f) = \theta_j(f)/\Delta d$. By sum up complex amplitude of different samples, wavenumber spectra $S(k, f)$ can be calculated, $S(k, f) = \frac{1}{M}\sum_{j=1}^{M} I_{(0,\Delta k)}[k - k^j(f)]|C^j_{XY}(f)|$.Thus, the wavenumber–frequency spectra $S(k, f)$ of potential fluctuations for radial position r=4.5cm in region I, II and III are shown in figure 4. Here, the (a), (b) and (c) represent the changes of the poloidal wavenumber ($k_\theta$) in the region I, II and III, and the (d), (e) and (f) represent the changes of the radial wavenumber ($k_r$) in the region I, II and III. *For region I*: in figure 4 (a) and (d), the

$m = 1$ at 0.5kGs, the $k_\theta$ is at ion diamagnetic direction (i-direction, the turbulence spatial scale $k_\theta \rho_S = k_\theta \frac{\sqrt{m_i T_e}}{eB} = k_\theta \frac{\sqrt{14\times1.66\times10^{-27}\times1.6\times10^{-19}T_e(eV)}}{1.6\times10^{-19}\cdot B} = 3.8\times10^{-4}\frac{k_\theta\sqrt{T_e(eV)}}{B} = 0.69$, $B = 0.5kGs$, $|k_\theta| < 60m^{-1}$, $T_e \approx 2.3eV$, $\rho_s = 0.0116m$), while the $k_r$ is outward as shown in figure 4 (d), and the frequency of the DW turbulence is below 10kHz, as shown in figure 4 (a) and (d) by the blue dashed lines. *For region II*: in figure 4 (b) and (e), the m increases to 2 at 1.0kGs, while the $k_\theta$ is at the electron diamagnetic direction (e-direction, the turbulence scale $k_\theta\rho_S = 0.5904 < 0.6$, $B = 1000Gs$, $|k_\theta| < 110m^{-1}$, $T_e \approx 2.4eV$, $\rho_s = 0.0054m$), while the $k_r$ is outward as shown in figure 4 (e), and the frequency of the DW turbulence expands to higher frequency range as shown in figure 4 (b) and (d). *For region III*: when the magnetic field increases continuously, the $m$ increases to 4 at 1.7kGs, the DW turbulence gradually transfers from ion diamagnetic direction to the electron diamagnetic direction and the absolute value of wavenumbers are much larger than that in region I and II, as shown in figure 4 (c). While, the $k_r$ indicates that the low frequency turbulence transport is still inward but the higher frequency turbulence transport is outward much, as shown in figure 4 (f).

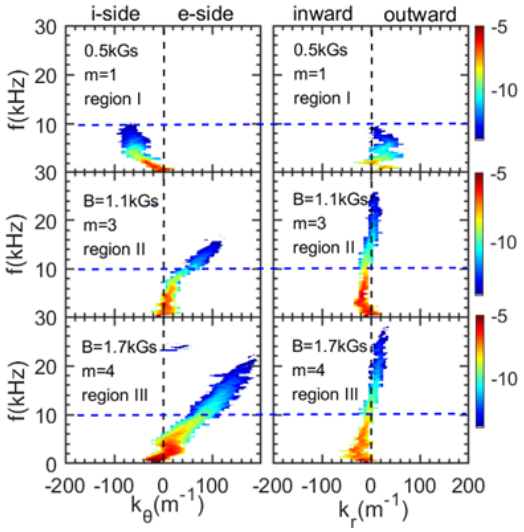


FIG. 4. Wavenumber–frequency spectra S(k, f) of the potential fluctuations at $r = 4.5cm$ for region I, II and III.

These results suggest that the low-frequency turbulence dominantly exists at low magnetic field at the ion diamagnetic direction. This is useful for the density increase since the diamagnetic effects as a finite pressure fluctuations to increase the total Reynolds force significantly[28]. While, with the magnetic field increase, the poloidal mode numbers increase from $m = 1$ to $m = 4$. It is clear that the turbulence frequency expends to more higher frequency and the turbulence propagation direction gradually reverses from i-side to e-side, as shown in figure 4 (b) and (c). The radial wavenumber spectra $S(k_r, f)$ suggest that the turbulence frequency also increases, and the low frequency component of the turbulence is outward, as shown in figure 4 (d). In figure 4 (e) and (f), the higher frequency component of the turbulence is outward and the low frequency component of the turbulence reverses to inward direction. These results show that the high-frequency turbulence with higher wavenumber dominantly reduces the density[29,30] and dissipates particle confinement.

In addition, the turbulence saturation phenomena at the steep density gradient region[31] is also observed when the magnetic field exceeds a critical magnetic field, which is defined due to the knee point of the density fluctuation curve, as shown in figure 5 (a) by the blue dashed line. Here, the fluctuation amplitude of the density is calculated from 4kHz to 20kHz at $r = 4.5cm$, corresponding to the steep density gradient region in figure 2 by the red line. An integral density and an integral temperature with different magnetic fields are obtained,

too, as shown in figure 5 (b). The integral regions are presented in figure 2 (a) and (b) by the black dashed lines, from $r = 1.5cm$ to 6cm in the ZPED. It is clear that the integral density decreases, but the temperature increases with the magnetic field increase with no external particle, heating and momentum source. One directly reason is that the magnetic field leads to the increase of the DW turbulence amplitude and reduces the particle confinement, until to the turbulence amplitude saturation at the steep density gradient. It is consistent with the results in the figure 4, as said the particle confinement dissipation with the increase of the wavenumber and the turbulence frequency, conversely, the temperature increases with the magnetic field increase. This means that an intrinsic evolution of the decoupling transport channel exists between the density and the temperature in a Cylindrical Laboratory Plasma Device. A relationship of the $\upsilon^*_{ee}$ versus to the $m$ is studied for a deep understanding of the intrinsic evolution of the DCD regime in this work, as shown in figure 5 (c). The $\upsilon^*_{ee}$ related to the $m$ at $r = 4.5cm$ is calculated by the $\upsilon^*_{ee} = \upsilon/\omega_p$, $\omega_p = \sqrt{\frac{4\pi n_e e^2}{m_e}}$ as shown in figure 5 (c)[32]. Here, the $\upsilon^*_{ee}$ is the normalized collision rate of the electron to electron, $\upsilon$ is the collision rate by the $\upsilon = 2.91 \times 10^{-6} n_e \ln\Lambda\ T_e^{-3/2} s^{-1}$ and the $\ln\Lambda = 23 - \ln(n_e^{\frac{1}{2}} T_e^{-\frac{3}{2}})$ at $T_e \leq 10eV$, the $\omega_p$ is the plasma frequency, the $n_e$ is the plasma density, the $e$ is the electronic charge and the $m_e$ is the electron mass, respectively. A change trend of the $\upsilon^*_{ee}$ versus to the $m$ in the three regions is shown in figure 5 (c) by the dotted ellipses. The $\upsilon^*_{ee}$ is almost no change while the $m$ increases in figure 5 (c) region I, and the $m$ stops increasing in figure 5 (c) in region II, and the $m$ is almost saturated and the $\upsilon^*_{ee}$ decreases in figure 5 (c) region III. These suggest that the low density due to the turbulence dissipation is one of the key points of the intrinsic evolution on the DCD regime of the density and the temperature. This is similar to the particle and temperature different transport channels of the H-mode and I-mode plasmas[33]. Actually, a few typical results on the $\upsilon^*_{ee}$ versus to the $m$ related to the H-mode and I-mode plasmas from different machines are evaluated statistically at $\rho = 0.95$, as shown in figure 5 (d). The data points are calculated based on the DIII-D, EAST, ASDEX-U and C-MOD. The red stars and the red circles represent the H-mode and the I-mode plasmas with different densities, respectively. The table 1 shows the $\upsilon^*_{ee}$, the $m$ and the $\langle n_e \rangle$. It is clear that the H-mode plasma density is larger than that in the I-mode case based on the data in the table 1. A regular shape of the $\upsilon^*_{ee}$ versus to the $m$ is almost similar to the results in figure 5 (c). This comparison result of the figure 5(c) and 5(d) identifies that the density is a key parameter of the intrinsic evolution for the DCD regime of the density and temperature in a Cylindrical Laboratory Plasma Device, similar to the different transport channels of the density and the temperature in the H-mode and the I-mode plasmas.

TABLE I. the details of the $\upsilon^*_{ee}(\times 10^{-2})$, the $m$ and the $\langle n_e \rangle(\times 10^{19} m^{-3})$ from a few tokamaks with H-mode and I-mode plasmas.

| | | DIII-D | EAST | ASDEX-U | C-MOD |
|---|---|---|---|---|---|
| $\upsilon^*_{ee}$ | H | 5.54[33] | 6.74[37] | 2.83[33,42] | 5.89[33] |
| | I | 7.34[33] | 6.09[38] | 2.79[33,42] | 3.58[19,33] |
| $m$ | H | 60[34] | 75[39–41] | 40[43,44] | 42[48,49] |
| | I | ∼70[19,35] | ∼75[38] | 75[45] | ∼70[19] |
| $\langle n_e \rangle$ | H | 5.5[36] | 3[40] | ∼5.0[46,47] | ∼26[50] |
| | I | 4.5[19] | ∼2.5[41] | ∼3.5[42] | ∼12[51] |

An intrinsic evolution on the DCD regime has been observed on ZPED with the magnetic field increase: first, the temperature gradient is almost no change while the density gradient increases in region I; second, both density and temperature gradient increase in region II; and then the density gradient is almost no change while the temperature gradient increases in region III. The turbulence frequency expends to higher frequency region, the turbulence propagation direction gradually reverses, and that the high-frequency tur-

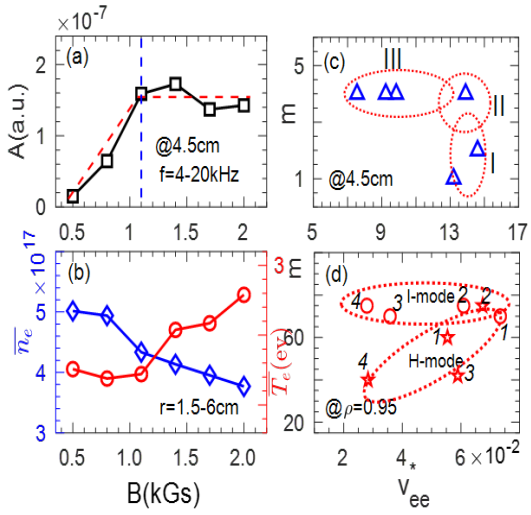


FIG. 5. (a) is the amplitudes of the density fluctuation with different magnetic field, the critical magnetic field is pointed by the blue dashed line. (b) shows the integral density and the temperature from $r = 1.5cm$ to $6cm$. (c) and (d) represent the relationship between the $v^*_{ee}$ and the $m$, respectively. The numbers 1-4 correspond to the data from the tokamaks DIII-D, EAST, ASDEX-U and C-MOD and the details are shown in Table 1.

bulence with higher wavenumber dominantly reduces the density and dissipates particle confinement. This is the element point to change the density. And, a regular shape of the $v^*_{ee}$ versus to the $m$ identifies that the density is a key parameter of the intrinsic evolution on the DCD regime of the density and the temperature in a cylindrical laboratory plasma device. It is similar to the different transport channels of the density and the temperature in the H-mode and the I-mode plasmas.

## ACKNOWLEDGMENTS

This work is supported by the National Natural Science Foundation of China (Grant No.11875234), the National Magnetic Confinement Fusion Science Program of China (2017YFE0301200, 2017YFE0301206 and 2017YFE0300500).

[1]Leigh Royden, Journal of Geophysical Research, Vol. 101, No. B8, 679-705, August 10 (1996)
[2]S.W.H. Cowley, E.J. Bunce, Planetary and Space Science 49 (2001) 1067–1088
[3]A. S. Bondarenko, et al., Nature Physics Vol 13 June, 2017
[4]N. V. Kabadi, et al., Physical Review E 104, L013201 (2021)
[5]Y. Ping, et al., Nature Physics, Vol 15 February, 2019, 138-141
[6]Dailey, C., Proceedings of the 6th Biennial AIAA/Northwestern University Gas Dynamics Symposium (1965)
[7]Martin, A. and R. Eskridge, Journal of Physics D: Applied Physics 38, 4168–4179 (2005)
[8]J. D. Callen and G. L. Jahns, Phys. Rev. Lett. 38, 491 (1977)
[9]D. L. Brower, et al., Physical Review Letters, Vol. 65, No. 3, 16 July (1990)
[10]G.M.D. Hogewe, J. Oroukke, and A.C.C. Sips, Plasma Physics and Controlled Fusion, Vol. 33. No. I. pp. 189-198 (1991)
[11]N. Deliyanakis, et al., Plasma Phys. Controlled Fusion 36 (1994) 1391-1406
[12]C. Hidalgo, et al., Physical Review Letters, Vol. 91, No. 6, 8 August (2003)
[13]G. R. Tynan, et al., Phys. Plasmas 8, 2691 (2001)
[14]F. Wagner et al, Phys. Rev Letters 53 (1984) 1453-6
[15]D.P. Schissel et al., Nucl. Fusion 34 1401 (1994)
[16]D. G. Whyte et al, Nuclear Fusion (2010) 105005
[17]A. E. Hubbard, et al., Phys. Plasmas 18, 056115 (2011)
[18]T Happel, et al., Plasma Phys. Control. Fusion 59 (2017) 014004
[19]A. Marinoni, et al., Nucl. Fusion 55 (2015) 093019

[20]A.E. White, et al., Nucl. Fusion 51 (2011) 113005 (9pp)
[21]P H Diamond, et al., Plasma Phys. Control. Fusion 53 124001(2011)
[22]W.W. Xiao, et al. (2019) AIP Advances 9 075026
[23]Rodney L. Burton and Susan G. DelMedicot, Journal of Propulsion and Power, Vol. 9, No. 5, Sept.-Oct. (1993)
[24]J. Wu, et al., Phys. Plasmas to be submitted
[25]M.N. Saha, Phil. Mag. 40, 472 (1920); Z. Phys. 6, 40 (1921)
[26]S.J. Levinson, et al. 1984 Nucl. Fusion 24 527
[27]Y. Ren, et al., Nucl. Fusion 53 083007 (2013)
[28]A. I. Smolyakov, et al., Phys. Plasmas, Vol. 7, No. 10, October 2000
[29]Z. Yan, et al., Phys. Rev. Lett. 112, 125002 (2014)
[30]C. Riccardi, X.T. Ding, M. Salierno, et al., Physics of Plasmas 4, 3749 (1997)
[31]F.D. Halpern and P. Ricci, Nucl. Fusion, 57 034001 (2017)
[32]A. V. Latyshev and A. A. Yushkanov, Theoretical and Mathematical Physics, 153 (2007)
[33]A.E. Hubbard,et al. (2016) Nucl. Fusion. 56,086003
[34]I. Holod, et al. (2015) Nucl. Fusion. 55,093020
[35]L. Schmitz, et al. (2008) Rev. Sci. Instrum. 79, 10F113
[36]S.R. Haskey, et al. (2022) Phys. Plasmas 29, 012506
[37]H.Q. Wang, et al. (2014) Nucl. Fusion. 54, 043014
[38]X. Feng,et al. (2019) Nucl. Fusion. 59,096025
[39]H.H. Wang, et al. (2020) Nucl. Fusion. 60, 126008
[40]X.Z. Gong, et al. (2017) Plasma Sci. Technol. 19, 032001
[41]Y.J. Liu, et al. (2020) Nucl. Fusion. 60, 082003
[42]F. Ryter, et al. (2017) Nucl. Fusion. 57,016004
[43]A. Mevedeva, et al. (2019) Plasma Phys. Control. Fusion. 61, 085011
[44]C.F. Maggi, et al. (2007) Nucl. Fusion. 47, 535
[45]P. Manz, et al. (2017) Nucl. Fusion. 57, 086022
[46]U. Plank, et al. (2019) 46th EPS Conference on Plasma Physics
[47]F. Ryter, et al. (2013) Nucl. Fusion. 53, 113003
[48]Y.Q. Huang, et al. (2020) Nucl. Fusion. 60,026014
[49]T. Golfinopoulos, et al. (2018) Nucl. Fusion. 58,056018
[50]A. Loarte, et al. (2011) Phys. Plasmas. 18, 056105
[51]M.L. Reinke, et al. (2019) Nucl. Fusion. 59, 046018